A defucosylated anti-CD44 monoclonal antibody 5-mG$_{2a}$-f exerts antitumor effects in mouse xenograft models of oral squamous cell carcinoma

JUNKO TAKEI[1,2*], MIKA K. KANEKO[1*], TOMOKAZU OHISHI[3*], HIDEKI HOSONO[1], TAKURO NAKAMURA[1], MIYUKI YANAKA[1], MASATO SANO[1], TEIZO ASANO[1], YUSUKE SAYAMA[1], MANABU KAWADA[3], HIROYUKI HARADA[2] and YUKINARI KATO[1,4]

[1]Department of Antibody Drug Development, Tohoku University Graduate School of Medicine, Aoba-ku, Sendai, Miyagi 980-8575; [2]Department of Oral and Maxillofacial Surgery, Graduate School of Medical and Dental Sciences, Tokyo Medical and Dental University, Bunkyo-ku, Tokyo 113-8510; [3]Institute of Microbial Chemistry (BIKAKEN), Numazu, Microbial Chemistry Research Foundation, Numazu-shi, Shizuoka 410-0301; [4]New Industry Creation Hatchery Center, Tohoku University, Sendai, Miyagi 980-8575, Japan

Received May 14, 2020; Accepted July 23, 2020

DOI: 10.3892/or.2020.7735

Abstract. CD44 is widely expressed on the surface of most tissues and all hematopoietic cells, and regulates many genes associated with cell adhesion, migration, proliferation, differentiation, and survival. CD44 has also been studied as a therapeutic target in several cancers. Previously, an anti-CD44 monoclonal antibody (mAb), C_{44}Mab-5 (IgG_1, kappa) was established by immunizing mice with CD44-overexpressing Chinese hamster ovary (CHO)-K1 cells. C_{44}Mab-5 recognized all CD44 isoforms, and showed high sensitivity for flow cytometry and immunohistochemical analysis in oral cancers. However, as the IgG_1 subclass of C_{44}Mab-5 lacks antibody-dependent cellular cytotoxicity (ADCC) and complement-dependent cytotoxicity (CDC), the antitumor activity of C_{44}Mab-5 could not be determined. In the present study, we converted the mouse IgG_1 subclass antibody C_{44}Mab-5 into an IgG_{2a} subclass antibody, 5-mG$_{2a}$, and further produced a defucosylated version, 5-mG$_{2a}$-f, using FUT8-deficient ExpiCHO-S (BINDS-09) cells. Defucosylation of 5-mG$_{2a}$-f was confirmed using fucose-binding lectins, such as AAL and PhoSL. The dissociation constants (K_D) for 5-mG$_{2a}$-f against SAS and HSC-2 oral cancer cells were determined through flow cytometry to be 2.8×10^{-10} M and 2.6×10^{-9} M, respectively, indicating that 5-mG$_{2a}$-f possesses extremely high binding affinity. Furthermore, immunohistochemical staining using 5-mG$_{2a}$-f specifically stained the membranes of oral cancer cells. *In vitro* analysis demonstrated that 5-mG$_{2a}$-f showed moderate ADCC and CDC activities against SAS and HSC-2 oral cancer cells. *In vivo* analysis revealed that 5-mG$_{2a}$-f significantly reduced tumor development in SAS and HSC-2 xenografts in comparison to control mouse IgG, even after injection seven days post-tumor inoculation. Collectively, these results suggest that treatment with 5-mG$_{2a}$-f may represent a useful therapy for patients with CD44-expressing oral cancers.

Correspondence to: Professor Yukinari Kato, New Industry Creation Hatchery Center, Tohoku University, 2-1 Seiryo-machi, Aoba-ku, Sendai, Miyagi 980-8575, Japan
E-mail: yukinarikato@med.tohoku.ac.jp

*Contributed equally

Abbreviations: AAL, *Aleuria aurantia* lectin; ABTU, Antibody Bank of Tohoku University; ADCC, antibody-dependent cellular cytotoxicity; ATCC, American Type Culture Collection; BSA, bovine serum albumin; CasMab, cancer-specific mAb; CBIS, cell-based immunization and screening; CDC, complement-dependent cytotoxicity; CD44s, CD44 standard; CD44v, CD44 variant; CHO, Chinese hamster ovary; Con A, concanavalin A; DMEM, Dulbecco's modified Eagle's medium; EDTA, ethylenediaminetetraacetic acid; ELISA, enzyme-linked immunosorbent assay; FBS, fetal bovine serum; FDA, Food and Drug Administration; FGF, fibroblast growth factor; HNSCC, head and neck squamous cell carcinoma; HB-EGF, heparin-binding epidermal growth factor; JCRB, Japanese Collection of Research Bioresources Cell Bank; mAb, monoclonal antibody; OSCC, oral squamous cell carcinoma; PBS, phosphate-buffered saline; PDPN, podoplanin; PhoSL, *Pholiota squarrosa* lectin; PODXL, podocalyxin; PVDF, polyvinylidene difluoride; RTKs, receptor tyrosine kinases; RT-PCR, reverse transcription-polymerase chain reaction; SCC, squamous cell carcinoma; SDS, sodium dodecyl sulfate; SEM, standard error of the mean; VEGFR, vascular endothelial growth factor receptor

Key words: CD44, monoclonal antibody, antibody-dependent cellular cytotoxicity, complement-dependent cytotoxicity, antitumor activity, oral cancer

Introduction

Oral cancers account for about 2% of all cancer cases diagnosed worldwide (1). More than 350,000 individuals are diagnosed with oral cancer every year, and oral cancers prove fatal for approximately 170,000 of these people. Major risk factors for

oral cancer include the use of alcohol and tobacco (2). Although decreased drinking and smoking have resulted in a decline in the incidence of oral cancer, recent studies have reported an increase in the number of young patients diagnosed with these diseases (3,4).

CD44 is known to be expressed in many cell types, including epithelial cells, fibroblasts, endothelial cells, and leukocytes (5). CD44 plays important roles in cell proliferation, adhesion, and migration (6). The CD44 gene consists of 20 exons (7). The smallest isoform is the standard form of CD44 (CD44s), which possesses 10 exons; other possible isoforms are categorized as CD44 variants (CD44v), which are generated by alternatively spliced transcripts (8). Post-translational modifications such as *N*- and *O*-glycosylation and heparan sulfate modification also augment the diversity of CD44 (9,10). Both CD44s and CD44v are overexpressed in many cancers; however, a pattern of expression remains to be elucidated.

One of the CD44 variants, CD44v6, was first identified as contributing to cancer metastasis, and CD44v6-specific monoclonal antibodies (mAbs) were found to inhibit metastasis of rat pancreatic cancers (11,12). Some CD44v6 isoforms act as co-receptors for receptor tyrosine kinases (RTKs) such as MET and vascular endothelial growth factor receptor (VEGFR)-2 (13-15). The transfection of CD44v4-7 cDNA confers a metastatic phenotype in non-metastatic cells (16). Another CD44 variant, CD44v3, binds to several heparan sulfate-binding growth factors such as fibroblast growth factors (FGFs) and heparin-binding epidermal growth factor (HB-EGF), and induces tumor progression (17,18). Several CD44 variants were also reported as prognostic markers in head and neck, lung, colorectal, breast, and hepatocellular cancers (19-23).

Many mAbs have been developed to target CD44 (24-26). mAbs that neutralize contact between hyaluronic acid and CD44 have been shown to inhibit anchorage-independent growth of murine mammary carcinoma cells and human colon carcinoma cells (24). Anti-CD44 mAbs were also found to exhibit significant antitumor activity in mouse xenograft models of human cancers (25,26). Previously, we established clone C_{44}Mab-5 (IgG_1, kappa) using Cell-Based Immunization and Screening (CBIS) (27). C_{44}Mab-5 recognized both CD44s and CD44v isoforms, and demonstrated high sensitivity for flow cytometry and immunohistochemical analysis in oral cancers. Because the IgG_1 subclass of C_{44}Mab-5 lacks antibody-dependent cellular cytotoxicity (ADCC) and complement-dependent cytotoxicity (CDC), antitumor activity of C_{44}Mab-5 could not be determined.

In this study, we converted the IgG_1 subclass C_{44}Mab-5 into a mouse IgG_{2a} subclass mAb, 5-mG_{2a}, and further produced a defucosylated version, 5-mG_{2a}-f, using FUT8-deficient ExpiCHO-S cells (28). We then investigated whether 5-mG_{2a}-f exhibited ADCC, CDC and antitumor activities against oral cancers.

Materials and methods

Cell lines. Oral squamous carcinoma cell lines including HSC-2 (oral cavity) and SAS (tongue) were obtained from the Japanese Collection of Research Bioresources Cell Bank (JCRB; Osaka, Japan). Chinese hamster ovary (CHO)-K1 was obtained from the American Type Culture Collection (ATCC). CD44v3-10 plus N-terminal PA16 tag-overexpressed CHO-K1 (CHO/PA16-CD44v3-10) was generated by transfection of pCAG/PA16-CD44v3-10 to CHO-K1 cells using the Neon Transfection System (Thermo Fisher Scientific, Inc.). The PA16 tag consists of 16 amino acids (GLEGGVAMPGAEDDVV) (27). HSC-2 and SAS cells were cultured in Dulbecco's modified Eagle's medium (DMEM; Nacalai Tesque, Inc.), and CHO-K1 and CHO/PA16-CD44v3-10 were cultured in RPMI-1640 medium (Nacalai Tesque, Inc.), supplemented with 10% heat-inactivated fetal bovine serum (FBS; Thermo Fisher Scientific Inc.), 100 units/ml of penicillin, 100 μg/ml streptomycin, and 0.25 μg/ml amphotericin B (Nacalai Tesque, Inc.) at 37˚C in a humidified atmosphere containing 5% CO_2.

Antibodies. Mouse anti-CD44s mAb C_{44}Mab-5 (IgG_1, kappa) was developed as previously described (27). Mouse IgG was purchased from Sigma-Aldrich Corp. (Merck KGaA). To generate recombinant C_{44}Mab-5 (recC_{44}Mab-5), cDNAs of C_{44}Mab-5 heavy and light chains were subcloned into pCAG-Neo and pCAG-Ble vectors (FUJIFILM Wako Pure Chemical Corporation), respectively. To generate 5-mG_{2a}-f, appropriate V_H cDNA of mouse C_{44}Mab-5 and C_H of mouse IgG_{2a} were subcloned into pCAG-Neo vector, and light chain of C_{44}Mab-5 was subcloned into pCAG-Ble vector. Vectors were transfected into ExpiCHO-S or BINDS-09 (FUT8-deficient ExpiCHO-S cells) using the ExpiCHO Expression System (28). recC_{44}Mab-5 and 5-mG_{2a}-f were purified using Protein G-Sepharose (GE Healthcare Bio-Sciences).

Animals. All animal experiments were performed in accordance with relevant guidelines (e.g. ARRIVE guidelines) and regulations (e.g. 3R regulations) to minimize animal suffering and distress in the laboratory (29,30). Seventy female BALB/c nude mice (6 weeks old, 15-18 g) were purchased from Charles River (Kanagawa, Japan). Animal studies for ADCC and antitumor activity were approved by the Institutional Committee for Experiments of the Institute of Microbial Chemistry (permit number: 2020-003). Mice were maintained in a pathogen-free environment (23±2˚C, 55±5% humidity) on 11 h light/13 h dark cycle with food and water supplied *ad libitum* during the experimental period. Mice were monitored for health and weight every 1 or 5 days. Experiment duration was three weeks. A bodyweight loss exceeding 25% and a maximum tumor size exceeding 3,000 mm^3 were identified as humane endpoints. Mice were euthanized by cervical dislocation, and the death was verified by respiratory arrest and cardiac arrest.

Enzyme-linked immunosorbent assay (ELISA). C_{44}Mab-5 and 5-mG_{2a}-f were immobilized on Nunc Maxisorp 96-well immunoplates (Thermo Fisher Scientific Inc.) at 1 μg/ml for 30 min. After blocking using SuperBlock buffer (Thermo Fisher Scientific Inc.) containing 0.5 mM $CaCl_2$, the plates were incubated with biotin-labeled lectins, such as *Aleuria aurantia* lectin (AAL; Vector Laboratories), *Pholiota squarrosa* lectin (PhoSL; J-OIL MILLS, Inc.) (31), and concanavalin A (ConA; Vector Laboratories), followed by 1:3,000 diluted peroxidase-conjugated streptavidin (Agilent Technologies). The enzymatic reaction was produced using a 1-Step Ultra

TMB-ELISA (Thermo Fisher Scientific Inc.). The optical density was measured at 655 nm using an iMark microplate reader (Bio-Rad Laboratories, Inc.).

Flow cytometry. Cells were harvested by brief exposure to 0.25% trypsin/1 mM ethylenediaminetetraacetic acid (EDTA; Nacalai Tesque, Inc.). After washing with 0.1% bovine serum albumin (BSA) in phosphate-buffered saline (PBS), cells were treated with primary mAbs for 30 min at 4˚C and subsequently with Alexa Fluor 488-conjugated anti-mouse IgG (1:1,000; Cell Signaling Technology, Inc.). Fluorescence microscopy data were collected using an EC800 Cell Analyzer (Sony Corp.).

Immunohistochemical analyses. Histologic sections (4-μm thick) of an oral cancer tissue microarray (catalogue number: OR481; US Biomax Inc.) were directly autoclaved in citrate buffer (pH 6.0; Agilent Technologies Inc.) for 20 min. Sections were then incubated with 1 μg/ml primary mAbs for 1 h at room temperature and treated using an Envision+ Kit (Agilent Technologies) for 30 min. Color was developed using 3,3'-diaminobenzidine tetrahydrochloride (DAB; Agilent Technologies Inc.) for 2 min, and sections were then counterstained with hematoxylin (FUJIFILM Wako Pure Chemical Corporation). Hematoxylin and eosin (H&E) staining (FUJIFILM Wako Pure Chemical Corporation) was performed using consecutive tissue sections. Leica DMD108 (Leica Microsystems GmbH) was used to examine the sections and obtain images.

Determination of the binding affinity. Cells were suspended in 100 μl of serially diluted mAbs (0.3 ng/ml-5 μg/ml), followed by the addition of Alexa Fluor 488-conjugated anti-mouse IgG (1:200; Cell Signaling Technology, Inc.). Fluorescence microscopy data were collected using an EC800 Cell Analyzer (Sony Corp.). The dissociation constant (K_D) was calculated by fitting binding isotherms to built-in one-site binding models in GraphPad PRISM 8 (GraphPad Software, Inc.).

Western blot analysis. Cell lysates (10 μg) were boiled in sodium dodecyl sulfate (SDS) sample buffer (Nacalai Tesque, Inc.). Proteins were separated on 5-20% polyacrylamide gels (FUJIFILM Wako Pure Chemical Corporation) and transferred onto polyvinylidene difluoride (PVDF) membranes (Merck KGaA). After blocking with 4% skim milk (Nacalai Tesque, Inc.) in PBS with 0.05% Tween 20, the membranes were incubated with 10 μg/ml of an anti-CD44 mAb [clone C_{44}Mab-46 (mouse IgG_1, kappa)]; available from Antibody Bank of Tohoku University (ABTU; Miyagi, Japan); http://www.med-tohoku-antibody.com/topics/001_paper_antibody_PDIS.htm#antiCD44) or 1 μg/ml of anti-β-actin (clone AC-15; cat. no. A5441; Sigma-Aldrich Corp.; Merck KGaA). This was followed by incubation with peroxidase-conjugated anti-mouse immunoglobulins (Agilent Technologies Inc.). Finally, protein bands were detected with ImmunoStar LD (FUJIFILM Wako Pure Chemical Corporation) using a Sayaca-Imager (DRC Co., Ltd.).

Reverse transcription-polymerase chain reaction (RT-PCR). Total RNAs were prepared from cell lines using an RNeasy Mini Prep Kit (Qiagen Inc.). The initial cDNA strand was synthesized using SuperScript IV Reverse Transcriptase (Thermo Fisher Scientific, Inc.) by priming nine random oligomers and an oligo(dT) primer according to the manufacturer's instructions. We performed 35 cycles of PCR for amplification using HotStarTaq DNA Polymerase (Qiagen Inc.) with 0.2 μM of primer sets: Human CD44 sense (5'-GAAAGGAGCAGC ACTTCAGG-3'), human CD44 antisense (5'-ACTGCAATG CAAACTGCAAGC-3'), GAPDH sense (5'-CAATGACCC CTTCATTGACC-3'), and GAPDH antisense (5'-GTCTTC TGGGTGGCAGTGAT-3').

ADCC. Six six-week-old female BALB/c nude mice were purchased from Charles River (Kanagawa, Japan). After euthanization by cervical dislocation, spleens were removed aseptically and single-cell suspensions obtained by forcing spleen tissues through a sterile cell strainer (352360, BD Falcon, Corning, Inc.) using a syringe. Erythrocytes were lysed with a 10-sec exposure to ice-cold distilled water. Splenocytes were washed with DMEM and resuspended in DMEM with 10% FBS and used as effector cells. Target cells were labeled with 10-μg/ml Calcein AM (Thermo Fisher Scientific, Inc.) and resuspended in the same medium. The target cells ($2x10^4$ cells/well) were plated in 96-well plates and mixed with effector cells, anti-CD44s antibodies, or control IgG (mouse IgG_{2a}) (Sigma-Aldrich Corp.; Merck KGaA). After a 5-h incubation, the Calcein AM release of supernatant from each well was measured. Fluorescence intensity was determined using a microplate reader (Power Scan HT) (BioTek Instruments) with an excitation wavelength of 485 nm and an emission wavelength of 538 nm. Cytolytic activity (as % of lysis) was calculated using the equation: % lysis=(E-S)/(M-S) x100, where E is the fluorescence of the combined target and effector cells, S is the spontaneous fluorescence of the target cells only, and M is the maximum fluorescence measured after lysing all cells with a buffer containing 0.5% Triton X-100, 10 mM Tris-HCl (pH 7.4), and 10 mM of EDTA.

CDC. Cells in DMEM supplemented with 10% FBS were plated in 96-well plates ($2x10^4$ cells/well), and incubated for 5 h at 37˚C with either anti-CD44s antibodies or control IgG (mouse IgG_{2a}) (Sigma-Aldrich Corp.; Merck KGaA) and 10% rabbit complement (Low-Tox-M Rabbit Complement; Cedarlane Laboratories). To assess cell viability, an MTS [3-(4,5-dimethylthiazol-2-yl)-5-(3-carboxymethoxyphenyl)-2-(4-sulfophenyl)-2H-tetrazolium; inner salt] assay was performed using a CellTiter 96®AQueous assay kit (Promega Corp.).

3D cell proliferation assay. 3D cell proliferation was measured with the CellTiter-Glo® 3D cell viability assay (Promega Corp.) according to the manufacturer's instructions. Briefly, the cells were plated (2,000 cells/100 μl/well) in triplicate in 96-well ultra low attachment plates (Corning Inc.) with PBS or 100 μg/ml of mouse IgG_{2a} and an anti-CD44 mAb (5-mG_{2a}-f) in DMEM containing 10% FBS. The cell viability was measured after 48 h of incubation. The CellTiter-Glo® 3D reagent was added into wells in a 1:1 dilution (100 μl volume in well:100 μl of reagent) and then the plates were shaken for 5 min on an orbital shaker and incubated at room temperature for an additional 25 min. The luminescent signal was read using an EnSpire multi-plate reader (Perkin Elmer). Images were taken

using an Evolution MP camera (Media Cybernetics). The proliferation rate was calculated relative to the control (PBS was added instead of the antibodies).

Antitumor activity of 5-mG$_{2a}$-f in the xenografts of oral cancers. Sixty-four six-week-old female BALB/c nude mice were purchased from Charles River (Kanagawa, Japan) and used at 10 weeks of age. HSC-2 and SAS cells (0.3 ml of 1.33x10^8 cells/ml in DMEM) were mixed with 0.5 ml BD Matrigel Matrix Growth Factor Reduced (BD Biosciences). One hundred microliters of this suspension (5x10^6 cells) was injected subcutaneously into the left flank. After day 1 (protocol-1) or day 7 (protocol-2), 100 μg of 5-mG$_{2a}$-f and control mouse IgG (Sigma-Aldrich Corp.; Merck KGaA) in 100 μl PBS were injected intraperitoneally (i.p.) into treated and control mice, respectively. Additional antibodies were then injected on days 7 and 14 (protocol-1) or on days 14 and 21 (protocol-2). Nineteen days (protocol-1) or 27 days (protocol-2) after cell implantation, all mice were euthanized by cervical dislocation and tumor diameters and volumes were determined as previously described (32).

Statistical analyses. All data are expressed as mean ± standard error of the mean (SEM). Statistical analysis was carried out using ANOVA following Tukey-Kramer's test for ADCC and CDC. Sidak's multiple comparisons test was used for tumor volume and mouse weight, or Welch's t test for tumor weight and 3D cell proliferation assay using GraphPad Prism 7 (GraphPad Software, Inc.). P<0.05 was adopted as a level of statistical significance.

Results

Production and characterization of 5-mG$_{2a}$-f, a core-fucose-deficient mouse IgG$_{2a}$-type anti-CD44 antibody. As mouse IgG$_{2a}$ possesses high ADCC and CDC activities (33), we first produced a mouse IgG$_{2a}$ version of mouse IgG$_1$ C$_{44}$Mab-5 by subcloning appropriate V$_H$ cDNA of C$_{44}$Mab-5 and C$_H$ of mouse IgG$_{2a}$ into pCAG-Neo vector, and light chain of C$_{44}$Mab-5 into pCAG-Ble vector. This IgG$_{2a}$-type of C$_{44}$Mab-5 is henceforth referred to as 5-mG$_{2a}$. We additionally produced a core-fucose-deficient type of 5-mG$_{2a}$, henceforth referred to as 5-mG$_{2a}$-f, using the BINDS-09 cell line (FUT8-knockout Expi-CHO-S cell line) (28). Defucosylation of 5-mG$_{2a}$-f was confirmed using lectins such as *Aleuria aurantia* lectin (AAL, fucose binder) (34) and *Pholiota squarrosa* lectin (PhoSL, core fucose binder) (31). Concanavalin A (ConA, mannose binder) (35) was used as a control. Both C$_{44}$Mab-5 and 5-mG$_{2a}$-f were detected using ConA (Fig. 1A). C$_{44}$Mab-5, but not 5-mG$_{2a}$-f, was detected using AAL (Fig. 1B) or PhoSL (Fig. 1C), indicating that 5-mG$_{2a}$-f was defucosylated.

We examined the sensitivity of 5-mG$_{2a}$-f in CHO cells expressing CD44v3-10 plus N-terminal PA16 tag (CHO/PA16-CD44v3-10) and in oral squamous cell carcinoma (OSCC) cell lines (SAS and HSC-2) using flow cytometry. Both C$_{44}$Mab-5 and 5-mG$_{2a}$-f reacted with CHO/PA16-CD44v3-10 cells (Fig. 2A), but not with CHO-K1 cells (Fig. 2B). Both C$_{44}$Mab-5 and 5-mG$_{2a}$-f reacted with SAS cells (Fig. 2C) and HSC-2 cells (Fig. 2D), indicating that both mAbs showed high sensitivity against SAS and HSC-2 cells.

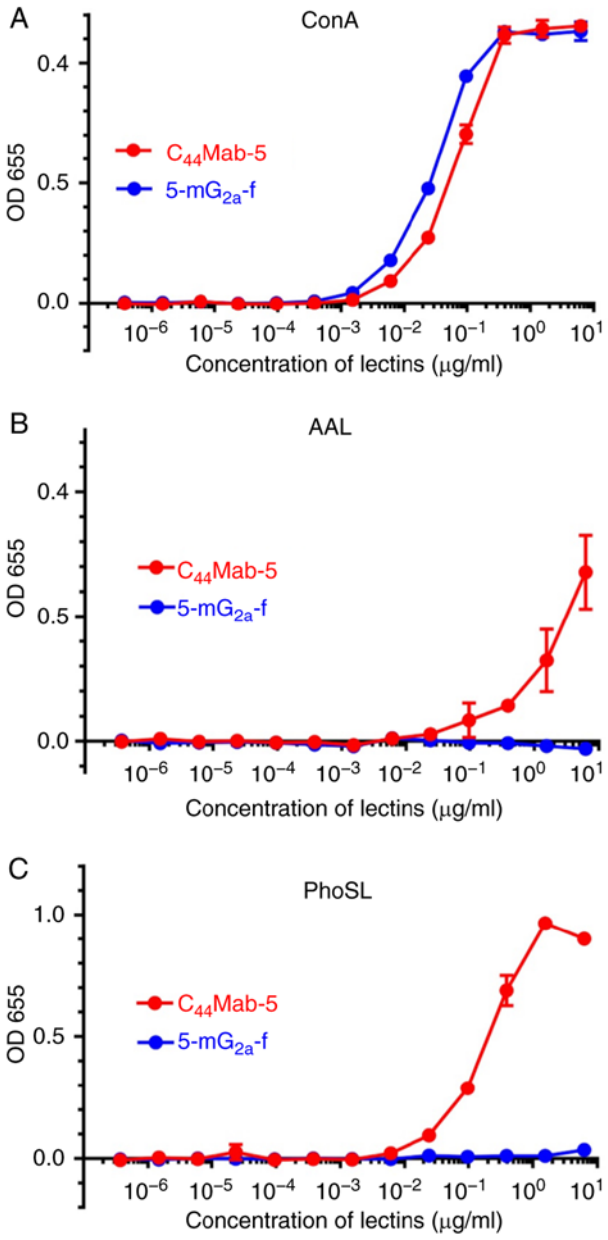

Figure 1. Confirmation of defucosylation of 5-mG$_{2a}$-f by enzyme-linked immunosorbent assay (ELISA) using lectins. (A) C$_{44}$Mab-5 and 5-mG$_{2a}$-f were immobilized and incubated with biotin-labeled concanavalin A (Con A), followed by peroxidase-conjugated streptavidin. The enzymatic reaction was produced using a 1-Step Ultra TMB-ELISA. (B) C$_{44}$Mab-5 and 5-mG$_{2a}$-f were immobilized and incubated with biotin-labeled *Aleuria aurantia* lectin (AAL), followed by peroxidase-conjugated streptavidin. The enzymatic reaction was produced using a 1-Step Ultra TMB-ELISA. (C) C$_{44}$Mab-5 and 5-mG$_{2a}$-f were immobilized and incubated with biotin-labeled *Pholiota squarrosa* lectin (PhoSL), followed by peroxidase-conjugated streptavidin. The enzymatic reaction was produced using a 1-Step Ultra TMB-ELISA.

As shown in Fig. S1A, CD44 was not detected by an anti-CD44s mAb (C$_{44}$Mab-46) in both SAS and HSC-2 cells presumably because the CD44 expression level in those cells might be low for the detection in western blot analysis. Then, we performed RT-PCR analysis for detection of CD44. As shown in Fig. S1B, the multiple bands of CD44v were detected in SAS and HSC-2 cells using PCR, indicating that CD44v is expressed in SAS and HSC-2 cells.

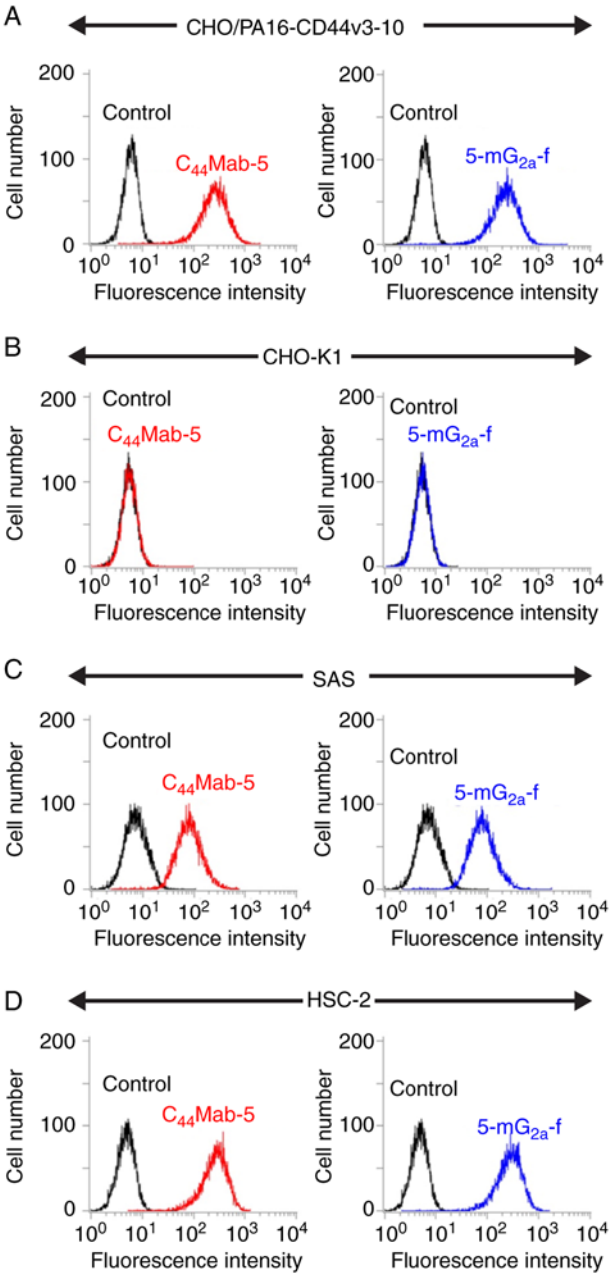

Figure 2. Flow cytometry using anti-CD44 mAbs. (A) CHO/PA16-CD44v3-10 cells were treated with C_{44}Mab-5 and 5-mG_{2a}-f (1 μg/ml), followed by secondary antibodies. (B) CHO-K1 cells were treated with C_{44}Mab-5 and 5-mG_{2a}-f (1 μg/ml), followed by secondary antibodies. (C) SAS cells were treated with C_{44}Mab-5 and 5-mG_{2a}-f (1 μg/ml), followed by secondary antibodies. (D) HSC-2 cells were treated with C_{44}Mab-5 and 5-mG_{2a}-f (1 μg/ml), followed by secondary antibodies. The black line represents the negative control. mAbs, monoclonal antibodies.

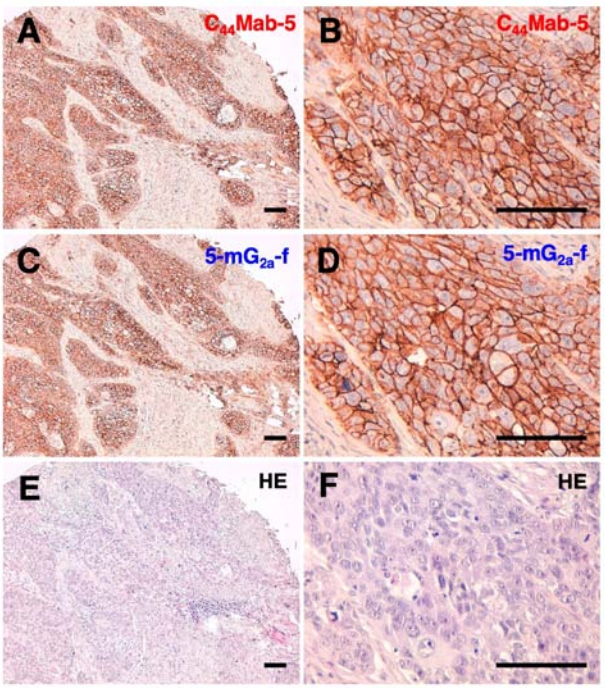

Figure 3. Immunohistochemical analysis using anti-CD44 mAbs against oral squamous cell carcinomas (OSCCs). (A and B) Consecutive tissue sections of OSCC were incubated with 1 μg/ml of C_{44}Mab-5 for 1 h at room temperature followed by treatment with an Envision+ kit for 30 min. Color was developed using DAB for 2 min, and sections were then counterstained with hematoxylin. (C and D) Consecutive tissue sections of OSCC were incubated with 1 μg/ml of 5-mG_{2a}-f for 1 h at room temperature followed by treatment with an Envision+ kit for 30 min. Color was developed using DAB for 2 min, and sections were then counterstained with hematoxylin. (E and F) Hematoxylin and eosin (HE) staining of consecutive tissue sections of OSCC. Scale bar, 100 μm. mAbs, monoclonal antibodies.

Next, we performed immunohistochemical analysis on oral cancer cell lines. Representative images are shown in Fig. 3. Both C_{44}Mab-5 (Fig. 3A and B) and 5-mG_{2a}-f (Fig. 3C and D) stained the plasma membrane of oral cancer cells. The sensitivity of 5-mG_{2a}-f was similar with that of C_{44}Mab-5. Both C_{44}Mab-5 and 5-mG_{2a}-f stained 33/38 cases (86.8%) of OSCCs of the tissue microarray. Hematoxylin & eosin (H&E) staining of consecutive tissue sections of OSCC is shown in Fig. 3E and F.

We performed a kinetic analysis of the interactions of recC_{44}Mab-5 and 5-mG_{2a}-f with SAS and HSC-2 oral cancer cell lines using flow cytometry. As shown in Fig. 4A, the dissociation constant (K_D) for recC_{44}Mab-5 in SAS cells was $2.4x10^{-10}$ M. In contrast, the K_D for 5-mG_{2a}-f in SAS cells was $2.8x10^{-10}$ M (Fig. 4A). The binding affinity of 5-mG_{2a}-f in SAS cells was very similar to that of recC_{44}Mab-5. Likewise, the K_D for recC_{44}Mab-5 against HSC-2 was $2.3x10^{-9}$ M (Fig. 4B). In contrast, the K_D for 5-mG_{2a}-f in HSC-2 cells was $2.6x10^{-9}$ M (Fig. 4B). The binding affinity of 5-mG_{2a}-f in HSC-2 cells was very similar to that of recC_{44}Mab-5. The binding affinity of 5-mG_{2a}-f in SAS was 9.3-fold higher than that against HSC-2.

ADCC and CDC activities of 5-mG_{2a}-f in oral cancer cell lines. Because the mouse IgG_1 subclass of C_{44}Mab-5 does not possess ADCC or CDC activities, we synthesized a mouse IgG_{2a} subclass mAb, and further defucosylated it to augment those activities. In this study, we examined whether the developed 5-mG_{2a}-f induced ADCC and CDC in CD44-expressing oral cancer cell lines, such as SAS and HSC-2 cells. As shown in Fig. 5A, 5-mG_{2a}-f exhibited higher ADCC (16% cytotoxicity) in SAS cells compared with that of control PBS (3.4% cytotoxicity; $P<0.01$) and control mouse IgG_{2a} treatment (4.2% cytotoxicity; $P<0.01$). Similarly, 5-mG_{2a}-f exhibited higher ADCC (18% cytotoxicity) against HSC-2 cells compared with that of control PBS (3.1% cytotoxicity; $P<0.01$) and control mouse IgG_{2a} treatment (5.2% cytotoxicity; $P<0.01$), indicating that ADCC in SAS cells is similar with that in HSC-2 cells,

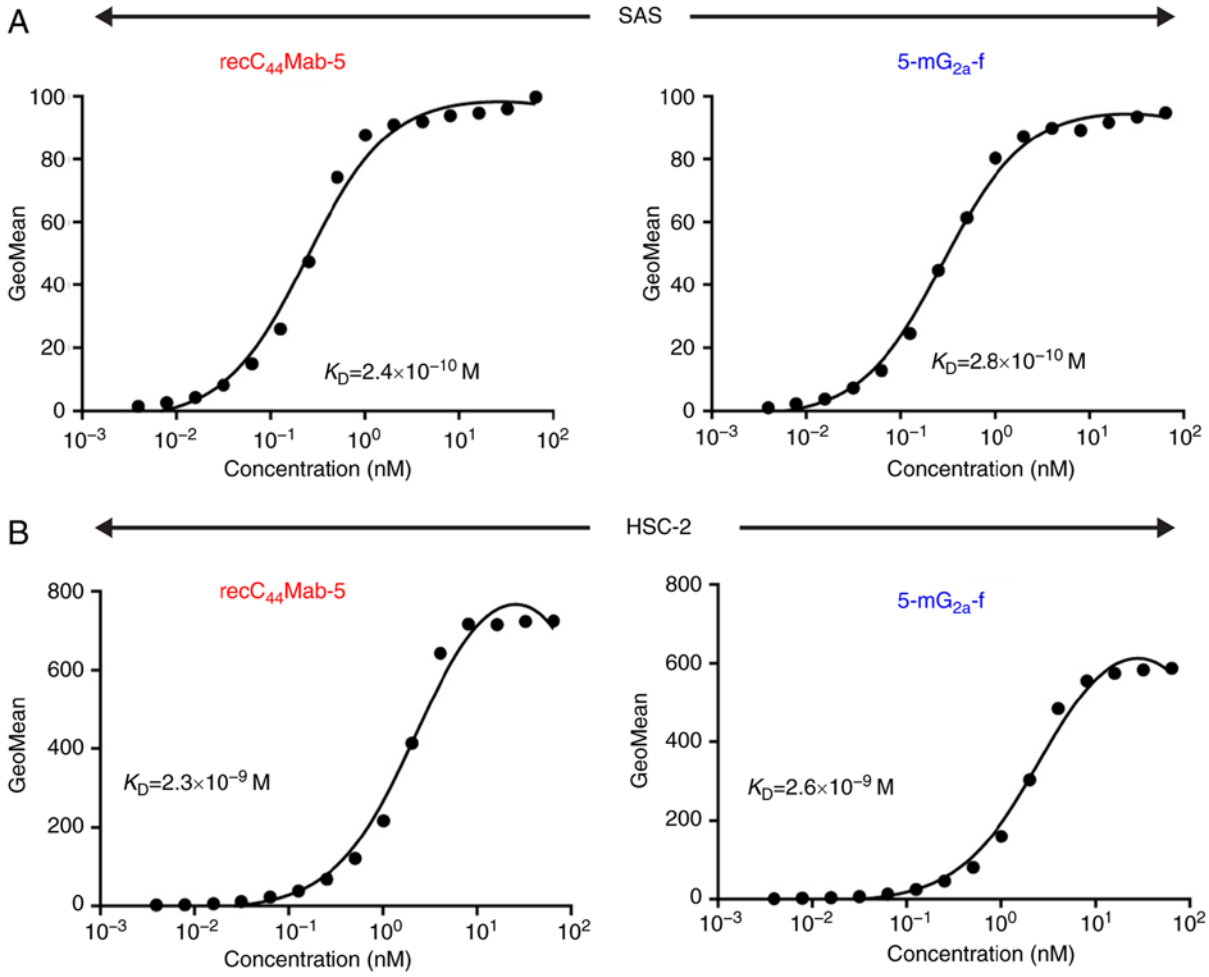

Figure 4. Determination of the binding affinity of anti-CD44 mAbs for oral cancer cells using flow cytometry. (A) SAS cells were suspended in 100 μl of serially diluted mAbs (0.3 ng/ml-5 μg/ml), followed by the addition of Alexa Fluor 488-conjugated anti-mouse IgG. Fluorescence data were collected using an EC800 Cell Analyzer. (B) HSC-2 cells were suspended in 100 μl of serially diluted mAbs (0.3 ng/ml-5 μg/ml), followed by the addition of Alexa Fluor 488-conjugated anti-mouse IgG. Fluorescence data were collected using an EC800 Cell Analyzer. K_D, dissociation constants; mAbs, monoclonal antibodies.

despite the binding affinity of 5-mG$_{2a}$-f in SAS cells being 9.3-fold higher than in HSC-2 cells (Fig. 4). As shown in Fig. 5B, 5-mG$_{2a}$-f exhibited slightly higher CDC (33% cytotoxicity) in SAS cells compared with control PBS (21% cytotoxicity; P<0.01) and control mouse IgG$_{2a}$ treatment (22% cytotoxicity; P<0.01). Similarly, 5-mG$_{2a}$-f exhibited slightly higher CDC (30% cytotoxicity) in HSC-2 cells compared with control PBS (18% cytotoxicity; P<0.01) and control mouse IgG$_{2a}$ treatment (19% cytotoxicity; not significant). Although ADCC/CDC activities of 5-mG$_{2a}$-f in oral cancer cells are not outstanding, 5-mG$_{2a}$-f may exert antitumor activity against oral cancer cells *in vivo*.

The influence of 5-mG$_{2a}$-f in oral cancer cell lines in anchorage-independent condition. Next, we investigated whether 5-mG$_{2a}$-f inhibits cell growth of SAS and HSC-2 cells in anchorage-independent condition. As shown in Fig. S2A, both SAS and HSC-2 cells grew in anchorage-independent condition for 48 h. In contrast, an anti-CD44 mAb (5-mG$_{2a}$-f) did not inhibit the growth of SAS or HSC-2 compared to control mouse IgG$_{2a}$ (Fig. S2B), indicating that 5-mG$_{2a}$-f did not affect the cell growth of oral cancer cell lines in anchorage-independent condition.

Antitumor activities of 5-mG$_{2a}$-f in the mouse xenografts of SAS oral cancer cells. SAS cells were subcutaneously implanted into the flanks of nude mice. In protocol-1, 5-mG$_{2a}$-f (100 μg) and control mouse IgG (100 μg) were injected i.p. three times into the mice, on days 1, 7, and 14 after SAS cell injections. Tumor volume was measured on days 6, 12, 15, and 19. Tumor development was significantly reduced in the 5-mG$_{2a}$-f-treated mice on days 12, 15, and 19 in comparison to the IgG-treated control mice (Fig. 6A). Tumor volume on day 19 was reduced by 27% after 5-mG$_{2a}$-f treatment. Tumors from 5-mG$_{2a}$-f-treated mice weighed significantly less than tumors from IgG-treated control mice (16.9% reduction, Fig. 6B). Resected tumors on day 19 are depicted in Fig. 6C. Control and 5-mG$_{2a}$-f-treated SAS xenograft mice are shown on day 19 in Fig. S3A and B, respectively. Total body weights did not significantly differ between the two groups (Fig. S3C).

In protocol-2 of the SAS xenograft models, tumor formation of 16 SAS-bearing mice was observed on day 7. Then, these 16 SAS-bearing mice were divided into a 5-mG$_{2a}$-f-treated group and a control group. On days 7, 14, and 21 after SAS cell injections into the mice, 5-mG$_{2a}$-f (100 μg) and control mouse IgG (100 μg) were injected i.p. into the mice. Tumor formation was observed in mice in both treated and control groups.

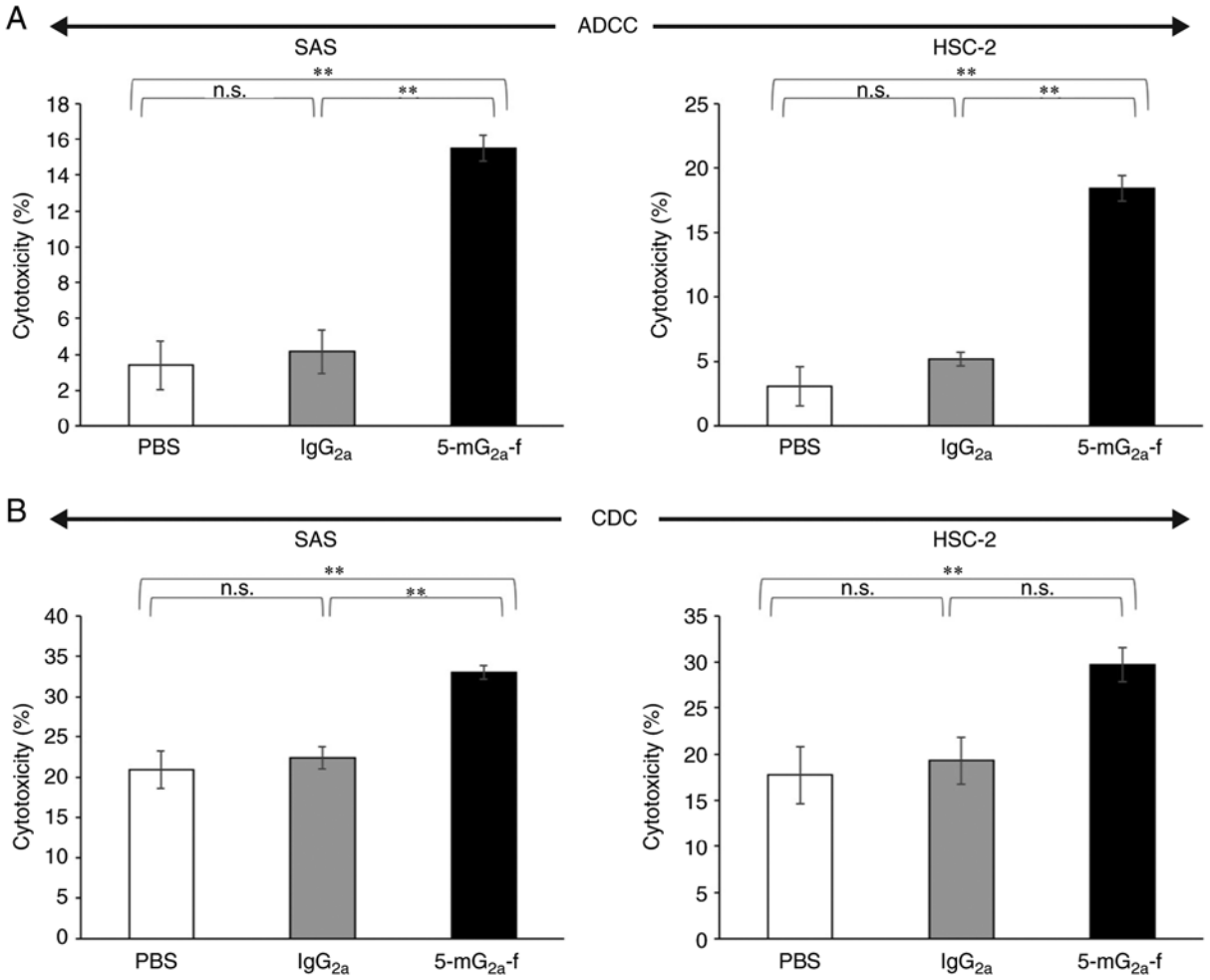

Figure 5. Evaluation of ADCC and CDC activities by 5-mG_{2a}-f. (A) ADCC activities by 5-mG_{2a}-f, control mouse IgG_{2a}, and control PBS in SAS and HSC-2 cells. (B) CDC activities by 5-mG_{2a}-f, control mouse IgG_{2a}, and control PBS in SAS and HSC-2 cells. Values are mean ± SEM. Asterisk indicates statistical significance (**P<0.01; n.s., not significant; ANOVA and Tukey-Kramer's test). ADCC, antibody-dependent cellular cytotoxicity; CDC, complement-dependent cytotoxicity.

Tumor volume was measured on days 7, 12, 15, 19, 22, and 27. 5-mG_{2a}-f-treated mice displayed significantly reduced tumor development on days 22 and 27 in comparison to IgG-treated control mice (Fig. 7A). Tumor volume reduction by 5-mG_{2a}-f was 43% on day 27. Tumors from the 5-mG_{2a}-f-treated mice weighed significantly less than tumors from the IgG-treated control mice (27.1% reduction, Fig. 7B). Resected tumors on day 27 are depicted in Fig. 7C. Control and 5-mG_{2a}-f-treated SAS xenograft mice are shown on day 27 in Fig. S4A and B, respectively. Total body weights did not significantly differ between the two groups (Fig. S4C). These results indicate that 5-mG_{2a}-f reduced the growth of SAS xenografts effectively, even when 5-mG_{2a}-f was injected 7 days post-SAS cell injections in mice.

Antitumor activities of 5-mG_{2a}-f in mouse xenografts of HSC-2 oral cancer cells. In a second xenograft model of oral cancers, HSC-2 cells were subcutaneously implanted into the flanks of nude mice. In protocol-1 of HSC-2 xenograft models, 5-mG_{2a}-f (100 μg) and control mouse IgG (100 μg) were injected i.p. three times into the mice, on days 1, 7, and 14 after HSC-2 cell injections into the mice. Tumor volume was measured on days 6, 12, 15, and 19. 5-mG_{2a}-f-treated mice displayed significantly reduced tumor development on days 12, 15, and 19 in comparison to IgG-treated control mice (Fig. 8A). Tumor volume reduction by 5-mG_{2a}-f was 53% on day 19. Tumors from 5-mG_{2a}-f-treated mice weighed significantly less than HSC-2 tumors from IgG-treated control mice (44.1% reduction, Fig. 8B). Resected tumors on day 19 are depicted in Fig. 8C. Control and 5-mG_{2a}-f-treated HSC-2 xenograft mice are shown on day 19 in Fig. S5A and B, respectively. Total body weights did not significantly differ between the two groups (Fig. S5C).

In protocol-2 of the HSC-2 xenograft models, tumor formation of 16 HSC-2-bearing mice was observed on day 7. Then, these 16 HSC-2-bearing mice were divided into a 5-mG_{2a}-f-treated group and a control group. On days 7, 14, and 21 after cell injections into the mice, 5-mG_{2a}-f (100 μg) and control mouse IgG (100 μg) were injected i.p. into the mice. Tumor volume was measured on days 7, 12, 15, 19, 22, and 27. 5-mG_{2a}-f-treated mice displayed significantly reduced tumor development on days 22 and 27 in comparison to IgG-treated control mice (Fig. 9A). Tumor volume reduction in 5-mG_{2a}-treated mice was 32% on day 27. Tumors from 5-mG_{2a}-f-treated mice weighed significantly less than tumors from IgG-treated control mice (27.1% reduction, Fig. 9B).

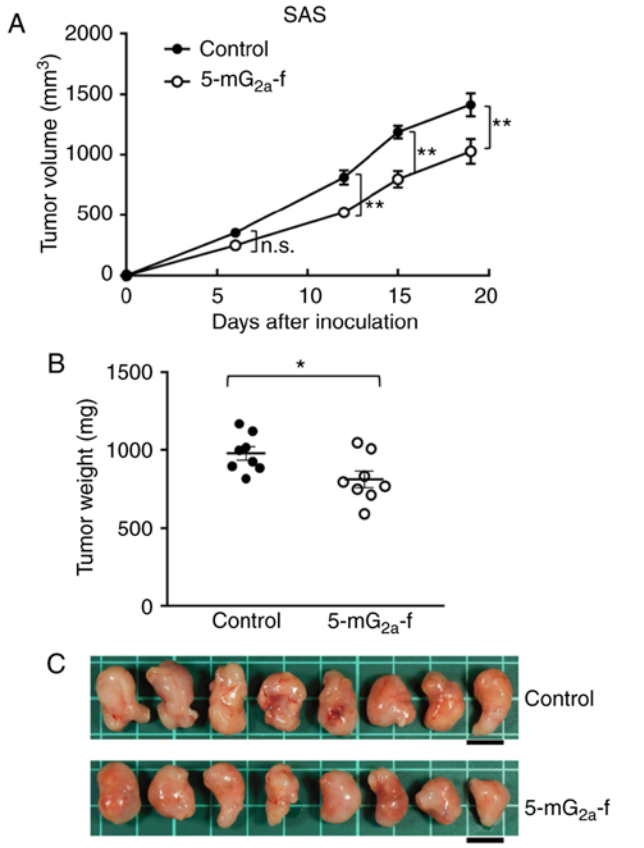

Figure 6. Evaluation of antitumor activity of 5-mG_{2a}-f (from day 1) in SAS xenografts. (A) SAS cells (5x10^6 cells) were injected subcutaneously into the left flank. After day 1, 100 μg of 5-mG_{2a}-f and control mouse IgG in 100 μl PBS were injected i.p. into treated and control mice, respectively. Additional antibodies were then injected on days 7 and 14. Tumor volume was measured on days 6, 12, 15, and 19. Values are mean ± SEM. Asterisk indicates statistical significance (**P<0.01; n.s., not significant; ANOVA and Sidak's multiple comparisons test). (B) Tumors of SAS xenografts were resected from 5-mG_{2a}-f and control mouse IgG groups. Tumor weight on day 19 was measured from excised xenografts. Values are mean ± SEM. Asterisk indicates statistical significance (*P<0.05, Welch's t test). (C) Resected tumors of SAS xenografts from 5-mG_{2a}-f and control mouse IgG groups on day 19. Scale bar, 1 cm.

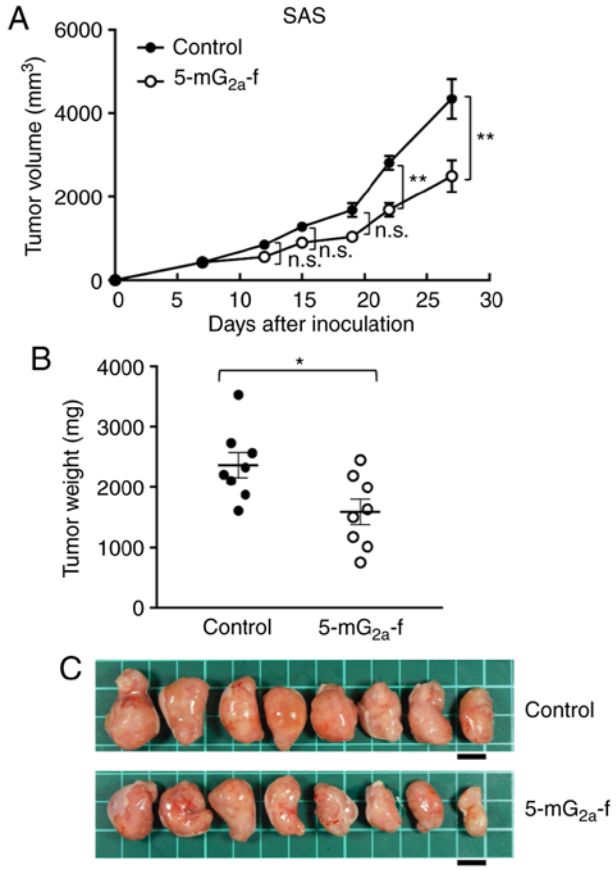

Figure 7. Evaluation of antitumor activity of 5-mG_{2a}-f (from day 7) in SAS xenografts. (A) SAS cells (5x10^6 cells) were injected subcutaneously into the left flank. After day 7, 100 μg of 5-mG_{2a}-f and control mouse IgG in 100 μl PBS were injected i.p. into treated and control mice, respectively. Additional antibodies were then injected on days 14 and 21. Tumor volume was measured on days 7, 12, 15, 19, 22, and 27. Values are mean ± SEM. Asterisk indicates statistical significance (**P<0.01; n.s., not significant; ANOVA and Sidak's multiple comparisons test). (B) Tumors of SAS xenografts were resected from 5-mG_{2a}-f and control mouse IgG groups. Tumor weight on day 27 was measured from excised xenografts. Values are mean ± SEM. Asterisk indicates statistical significance (*P<0.05, Welch's t test). (C) Resected tumors of SAS xenografts from 5-mG_{2a}-f and control mouse IgG groups on day 27. Scale bar, 1 cm.

Resected tumors on day 27 are depicted in Fig. 9C. Control and 5-mG_{2a}-f-treated HSC-2 xenograft mice are shown on day 27 in Fig. S6A and B, respectively. Total body weights did not significantly differ between the two groups (Fig. S6C). These results indicate that 5-mG_{2a}-f reduced the growth of HSC-2 xenografts effectively, even when 5-mG_{2a}-f was injected 7 days post-HSC-2 cell injections in mice.

Discussion

In the present study, we investigated whether anti-CD44 mAbs are advantageous for the treatment of oral cancers. We previously developed a sensitive and specific anti-CD44 mAb, C_{44}Mab-5, but were unable to demonstrate antitumor activity because the IgG_1 subclass does not possess ADCC/CDC activities (27). In this study, we developed this antibody into an IgG_{2a} subclass antibody, and augmented ADCC activity using a defucosylated variant. Oral cancers comprise several histological tumor types, such as squamous cell carcinoma (SCC), adenocarcinoma, mucoepidermoid carcinoma, and adenoid cystic carcinoma. Among these, SCC accounts for over 90% of all oral cancers (36). Therefore, we used SAS and HSC-2 cell lines, which are derived from SCC, and investigated ADCC/CDC and antitumor activities.

The most effective treatment of OSCC depends upon its clinical stage. Stage-I and -II (early stages) are treated via surgery or radiotherapy alone. In contrast, stage-III and -IV (advanced stages) require a combination of surgery, radiotherapy, and chemotherapy (37). For chemotherapy of OSCCs, cisplatin is mainly used, and is often combined with docetaxel and 5-fluorouracil (38,39). Other anticancer agents, such as paclitaxel, carboplatin, and methotrexate can be also used for OSCCs (40), but effective molecular targeting drugs, such as antibody therapies, are limited.

Recently, cetuximab, a mouse-human chimeric mAb (IgG_1) that targets epidermal growth factor receptor (EGFR), was approved by the Food and Drug Administration (FDA) in the USA for treatment of oral cancers (41). Cetuximab has been shown effective against locoregionally advanced head

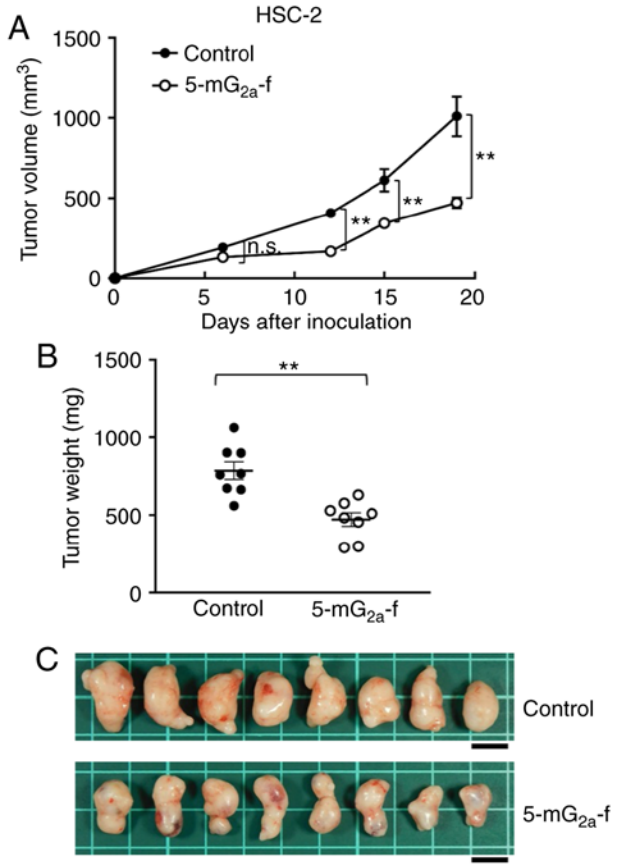

Figure 8. Evaluation of antitumor activity of 5-mG_{2a}-f (from day 1) in HSC-2 xenografts. (A) HSC-2 cells ($5x10^6$ cells) were injected subcutaneously into the left flank. After day 1, 100 μg of 5-mG_{2a}-f and control mouse IgG in 100 μl PBS were injected i.p. into treated and control mice, respectively. Additional antibodies were then injected on days 7 and 14. Tumor volume was measured on days 6, 12, 15, and 19. Values are mean ± SEM. Asterisk indicates statistical significance (**P<0.01; n.s., not significant, ANOVA and Sidak's multiple comparisons test). (B) Tumors of HSC-2 xenografts were resected from 5-mG_{2a}-f and control mouse IgG groups. Tumor weight on day 19 was measured from excised xenografts. Values are mean ± SEM. Asterisk indicates statistical significance (**P<0.01, Welch's t test). (C) Resected tumors of HSC-2 xenografts from 5-mG_{2a}-f and control mouse IgG groups on day 19. Scale bar, 1 cm.

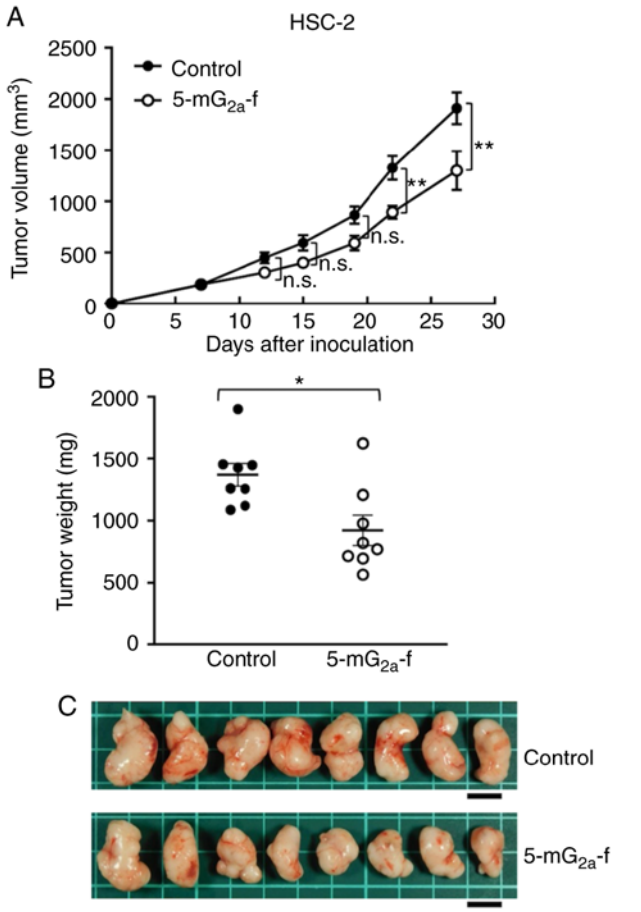

Figure 9. Evaluation of antitumor activity of 5-mG_{2a}-f (from day 7) in HSC-2 xenografts. (A) HSC-2 cells ($5x10^6$ cells) were injected subcutaneously into the left flank. After day 7, 100 μg of 5-mG_{2a}-f and control mouse IgG in 100 μl PBS were injected i.p. into treated and control mice, respectively. Additional antibodies were then injected on days 14 and 21. Tumor volume was measured on days 7, 12, 15, 19, 22, and 27. Values are mean ± SEM. Asterisk indicates statistical significance (**P<0.01; n.s., not significant; ANOVA and Sidak's multiple comparisons test). (B) Tumors of HSC-2 xenografts were resected from 5-mG_{2a}-f and control mouse IgG groups. Tumor weight on day 27 was measured from excised xenografts. Values are mean ± SEM. Asterisk indicates statistical significance (*P<0.05, Welch's t test). (C) Resected tumors of HSC-2 xenografts from 5-mG_{2a}-f and control mouse IgG groups on day 27. Scale bar, 1 cm.

and neck cancer and recurrent or metastatic squamous cell carcinoma of the head and neck (41-43). Although advances in diagnosis and therapeutic techniques have improved the overall 5-year survival rate to 70%, the 5-year survival rate in stage IV is only 40%; therefore, further treatments must be developed (44). In our recent study, we also developed a sensitive and specific mAb (EMab-17) against EGFR, and demonstrated its ADCC/CDC and antitumor activity against SAS and HSC-2 xenografts (32). Although we showed that EMab-17 could potentially be used for antibody-based therapy for EGFR-expressing OSCC, the difference between cetuximab and EMab-17 has not been clarified. Several studies characterizing EMab-17, including epitope mapping and signal induction in OSCC cells, are currently ongoing.

In another recent study, HER2 was shown to be expressed in oral cancers, and an anti-HER2 mAb (H_2Mab-19) demonstrated antitumor activity (45). Therefore, anti-HER2 therapies using trastuzumab could be effective for the treatment of oral cancers. HER2 expression was reported in only 1.4% of immunohistochemical analyses of oral cancer (46), although it is expressed in 10.4% of breast cancers (47). Therefore, targeting only HER2 may be insufficient for conquering oral cancers. As antitumor effects of combined gefitinib and trastuzumab or cetuximab and trastuzumab treatment on head and neck SCC (HNSCC) were demonstrated *in vitro* (48,49), those few oral cancer patients displaying HER2 overexpression/amplification may possibly benefit from anti-HER2 therapy.

Furthermore, we previously investigated whether podocalyxin (PODXL) may be a therapeutic target in OSCC using anti-PODXL mAbs (50). We engineered an anti-PODXL mAb of IgG_1 subclass (PcMab-47) into a mouse IgG_{2a}-type mAb (47-mG_{2a}) to increase ADCC. We further developed 47-mG2a-f, a core fucose-deficient variant of 47-mG_{2a} to further augment its ADCC. *In vivo* analysis revealed that 47-mG_{2a}-f, but not 47-mG_{2a}, exhibited antitumor activity in SAS and HSC-2 xenograft models at a dose of 100 μg/mouse/week administered three times. Although both 47-mG_{2a} and 47-mG_{2a}-f exhibited

antitumor activity in HSC-2 xenograft models at a dose of 500 μg/mouse/week administered twice, 47-mG_{2a}-f also demonstrated higher antitumor activity than 47-mG_{2a}, indicating that a core fucose-deficient anti-PODXL mAb could be useful for antibody-based therapy against PODXL-expressing OSCCs. Therefore, we used the core-fucose-deficient anti-CD44 mAb (5-mG_{2a}-f) for treating CD44-expressing oral cancers.

In this study, we demonstrated that 5-mG_{2a}-f exerts ADCC/CDC activities *in vitro*, and antitumor activities *in vivo*. Importantly, 5-mG_{2a}-f effectively reduced the growth of SAS and HSC-2 xenografts, even when 5-mG_{2a}-f was injected 7 days after cell implantations into the mice. However, tumor volume reduction of SAS and HSC-2 on day 27 by 5-mG_{2a}-f was still only 43 and 32%, respectively, indicating that anti-CD44 therapy might not be robust enough for conquering most oral cancers. One potential reason for this weak antitumor activity is the lower ADCC activity and CDC activity of 5-mG_{2a}-f, despite high binding activity in SAS cells (K_D: 2.8x10^{-10} M) and HSC-2 cells (K_D: 2.6x10^{-9} M).

In our previous report, C_{44}Mab-5 detected CD44s (27). Although the binding epitope of C_{44}Mab-5 may potentially be located between exon-1 and exon-5, we have not been able to determine the exact binding epitope of C_{44}Mab-5, likely because C_{44}Mab-5 recognizes the tertiary structure of CD44 rather simple peptides or glycans. Because the binding epitope is critical for ADCC/CDC activities of mAbs, other anti-CD44 mAbs of various epitopes will need to be developed in future studies.

Targeting multiple targets, such as EGFR, HER2, PODXL, and CD44 may be needed for effective therapy to conquer oral cancers. Another important goal is the targeting of cancer-specific antigens using a cancer-specific mAb (CasMab) because EGFR, HER2, PODXL, and CD44 are widely expressed in normal tissues. We previously established CasMab against podoplanin (PDPN), which is expressed in many cancers, including oral cancers (51-54). In xenograft models with HSC-2 cells, a mouse-human chimeric mAb, chLpMab-23, exerted antitumor activity using human natural killer cells, indicating that chLpMab-23 may be useful for antibody therapy against PDPN-expressing oral cancers (54). In the future study, cancer-specific anti-CD44 mAbs may also be developed that can reduce the adverse effects of traditional antibody therapy.

Acknowledgements

We thank Ms. Saori Handa and Mr. Yu Komatsu (Department of Antibody Drug Development, Tohoku University Graduate School of Medicine) for technical assistance concerning the *in vitro* experiments, and Ms. Akiko Harakawa [Institute of Microbial Chemistry (BIKAKEN), Numazu, Microbial Chemistry Research Foundation] for technical assistance regarding the animal experiments.

Funding

This research was supported in part by Japan Agency for Medical Research and Development (AMED) under grant nos. JP20am0401013 (YK), JP20am0101078 (YK), and JP20ae0101028 (YK), and by the Japan Society for the Promotion of Science (JSPS) Grants-in-Aid for Scientific Research (KAKENHI) grant nos. 17K07299 (MKK), 19K07705 (YK), and 20K16322 (MS).

Availability of data and materials

The datasets used and/or analyzed during the study are available from the corresponding author on reasonable request.

Authors' contributions

HHo, JT, TO, TN, MS, TA, YS, and MY performed the experiments. MKK analyzed the experimental data. MK, HHa, and YK designed the current study and wrote the manuscript. All authors read and approved the manuscript and agree to be accountable for all aspects of the research in ensuring that the accuracy or integrity of any part of the work are appropriately investigated and resolved.

Ethics approval and consent to participate

Animal studies for ADCC and the antitumor activity were approved by the Institutional Committee for Experiments of the Institute of Microbial Chemistry (Numazu-shi, Shizuoka, Japan) (permit no. 2020-003).

Patient consent for publication

Not applicable.

Competing interests

The authors declare that they have no competing interests.

References

1. Bray F, Ferlay J, Soerjomataram I, Siegel RL, Torre LA and Jemal A: Global cancer statistics 2018: GLOBOCAN estimates of incidence and mortality worldwide for 36 cancers in 185 countries. CA Cancer J Clin 68: 394-424, 2018.
2. Hashibe M, Brennan P, Chuang SC, Boccia S, Castellsague X, Chen C, Curado MP, Dal Maso L, Daudt AW, Fabianova E, *et al*: Interaction between tobacco and alcohol use and the risk of head and neck cancer: Pooled analysis in the international head and neck cancer epidemiology consortium. Cancer Epidemiol Biomarkers Prev 18: 541-550, 2009.
3. Tota JE, Anderson WF, Coffey C, Califano J, Cozen W, Ferris RL, St John M, Cohen EE and Chaturvedi AK: Rising incidence of oral tongue cancer among white men and women in the United States, 1973-2012. Oral Oncol 67: 146-152, 2017.
4. Hussein AA, Helder MN, de Visscher JG, Leemans CR, Braakhuis BJ, de Vet HCW and Forouzanfar T: Global incidence of oral and oropharynx cancer in patients younger than 45 years versus older patients: A systematic review. Eur J Cancer 82: 115-127, 2017.
5. Sherman L, Sleeman J, Herrlich P and Ponta H: Hyaluronate receptors: Key players in growth, differentiation, migration and tumor progression. Curr Opin Cell Biol 6: 726-733, 1994.
6. Slevin M, Krupinski J, Gaffney J, Matou S, West D, Delisser H, Savani RC and Kumar S: Hyaluronan-mediated angiogenesis in vascular disease: Uncovering RHAMM and CD44 receptor signaling pathways. Matrix Biol 26: 58-68, 2007.
7. Rodrigo JP, Dominguez F, Alvarez C, Gonzalez MV, Herrero A and Suárez C: Clinicopathologic significance of expression of CD44s and CD44v6 isoforms in squamous cell carcinoma of the supraglottic larynx. Am J Clin Pathol 118: 67-72, 2002.
8. Zöller M: CD44: Can a cancer-initiating cell profit from an abundantly expressed molecule? Nat Rev Cancer 11: 254-267, 2011.

9. Greenfield B, Wang WC, Marquardt H, Piepkorn M, Wolff EA, Aruffo A and Bennett KL: Characterization of the heparan sulfate and chondroitin sulfate assembly sites in CD44. J Biol Chem 274: 2511-2517, 1999.
10. Skelton TP, Zeng C, Nocks A and Stamenkovic I: Glycosylation provides both stimulatory and inhibitory effects on cell surface and soluble CD44 binding to hyaluronan. J Cell Biol 140: 431-446, 1998.
11. Hofmann M, Rudy W, Zöller M, Tölg C, Ponta H, Herrlich P and Günthert U: CD44 splice variants confer metastatic behavior in rats: Homologous sequences are expressed in human tumor cell lines. Cancer Res 51: 5292-5297, 1991.
12. Günthert U, Hofmann M, Rudy W, Reber S, Zöller M, Haussmann I, Matzku S, Wenzel A, Ponta H and Herrlich P: A new variant of glycoprotein CD44 confers metastatic potential to rat carcinoma cells. Cell 65: 13-24, 1991.
13. Tremmel M, Matzke A, Albrecht I, Laib AM, Olaku V, Ballmer-Hofer K, Christofori G, Héroult M, Augustin HG, Ponta H and Orian-Rousseau V: A CD44v6 peptide reveals a role of CD44 in VEGFR-2 signaling and angiogenesis. Blood 114: 5236-5244, 2009.
14. Orian-Rousseau V, Morrison H, Matzke A, Kastilan T, Pace G, Herrlich P and Ponta H: Hepatocyte growth factor-induced Ras activation requires ERM proteins linked to both CD44v6 and F-actin. Mol Biol Cell 18: 76-83, 2007.
15. Orian-Rousseau V, Chen L, Sleeman JP, Herrlich P and Ponta H: CD44 is required for two consecutive steps in HGF/c-Met signaling. Genes Dev 16: 3074-3086, 2002.
16. Rudy W, Hofmann M, Schwartz-Albiez R, Zöller M, Heider KH, Ponta H and Herrlich P: The two major CD44 proteins expressed on a metastatic rat tumor cell line are derived from different splice variants: Each one individually suffices to confer metastatic behavior. Cancer Res 53: 1262-1268, 1993.
17. Jackson DG, Bell JI, Dickinson R, Timans J, Shields J and Whittle N: Proteoglycan forms of the lymphocyte homing receptor CD44 are alternatively spliced variants containing the v3 exon. J Cell Biol 128: 673-685, 1995.
18. Bennett KL, Jackson DG, Simon JC, Tanczos E, Peach R, Modrell B, Stamenkovic I, Plowman G and Aruffo A: CD44 isoforms containing exon V3 are responsible for the presentation of heparin-binding growth factor. J Cell Biol 128: 687-698, 1995.
19. Hu S, Wu X, Zhou B, Xu Z, Qin J, Lu H, Lv L, Gao Y, Deng L, Yin J and Li G: IMP3 combined with CD44s, a novel predictor for prognosis of patients with hepatocellular carcinoma. J Cancer Res Clin Oncol 140: 883-893, 2014.
20. Auvinen P, Tammi R, Kosma VM, Sironen R, Soini Y, Mannermaa A, Tumelius R, Uljas E and Tammi M: Increased hyaluronan content and stromal cell CD44 associate with HER2 positivity and poor prognosis in human breast cancer. Int J Cancer 132: 531-539, 2013.
21. Fang YJ, Zhang L, Wu XJ, Lu ZH, Li JB, Ou QJ, Zhang MF, Ding PR, Pan ZZ and Wan DS: Impact of ERβ and CD44 expression on the prognosis of patients with stage II colon cancer. Tumour Biol 33: 1907-1914, 2012.
22. Kokko LL, Hurme S, Maula SM, Alanen K, Grénman R, Kinnunen I and Ventelä S: Significance of site-specific prognosis of cancer stem cell marker CD44 in head and neck squamous-cell carcinoma. Oral Oncol 47: 510-516, 2011.
23. Nguyen VN, Mirejovský T, Melinová L and Mandys V: CD44 and its v6 spliced variant in lung carcinomas: Relation to NCAM, CEA, EMA and UP1 and prognostic significance. Neoplasma 47: 400-408, 2000.
24. Ghatak S, Misra S and Toole BP: Hyaluronan oligosaccharides inhibit anchorage-independent growth of tumor cells by suppressing the phosphoinositide 3-kinase/Akt cell survival pathway. J Biol Chem 277: 38013-38020, 2002.
25. Marangoni E, Lecomte N, Durand L, de Pinieux G, Decaudin D, Chomienne C, Smadja-Joffe F and Poupon MF: CD44 targeting reduces tumour growth and prevents post-chemotherapy relapse of human breast cancers xenografts. Br J Cancer 100: 918-922, 2009.
26. Jin L, Hope KJ, Zhai Q, Smadja-Joffe F and Dick JE: Targeting of CD44 eradicates human acute myeloid leukemic stem cells. Nat Med 12: 1167-1174, 2006.
27. Yamada S, Itai S, Nakamura T, Yanaka M, Kaneko MK and Kato Y: Detection of high CD44 expression in oral cancers using the novel monoclonal antibody, C_{44}Mab-5. Biochem Biophys Rep 14: 64-68, 2018.
28. Kato Y, Mizuno T, Yamada S, Nakamura T, Itai S, Yanaka M, Sano M and Kaneko MK: Establishment of P38Bf, a core-fucose-deficient mouse-canine chimeric antibody against dog podoplanin. Monoclon Antib Immunodiagn Immunother 37: 218-223, 2018.
29. Kilkenny C, Browne WJ, Cuthill IC, Emerson M and Altman DG: Improving bioscience research reporting: The ARRIVE guidelines for reporting animal research. PLoS Biol 8: e1000412, 2010.
30. Aske KC and Waugh CA: Expanding the 3R principles: More rigour and transparency in research using animals. EMBO Rep 18: 1490-1492, 2017.
31. Kobayashi Y, Tateno H, Dohra H, Moriwaki K, Miyoshi E, Hirabayashi J and Kawagishi H: A novel core fucose-specific lectin from the mushroom *Pholiota squarrosa*. J Biol Chem 287: 33973-33982, 2012.
32. Takei J, Kaneko MK, Ohishi T, Kawada M, Harada H and Kato Y: A novel anti-EGFR monoclonal antibody (EMab-17) exerts antitumor activity against oral squamous cell carcinomas via antibody-dependent cellular cytotoxicity and complement-dependent cytotoxicity. Oncol Lett 19: 2809-2816, 2020.
33. Kato Y, Kunita A, Fukayama M, Abe S, Nishioka Y, Uchida H, Tahara H, Yamada S, Yanaka M, Nakamura T, *et al*: Antiglycopeptide mouse monoclonal antibody LpMab-21 exerts antitumor activity against human podoplanin through antibody-dependent cellular cytotoxicity and complement-dependent cytotoxicity. Monoclon Antib Immunodiagn Immunother 36: 20-24, 2017.
34. Wimmerova M, Mitchell E, Sanchez JF, Gautier C and Imberty A: Crystal structure of fungal lectin: Six-bladed beta-propeller fold and novel fucose recognition mode for *Aleuria aurantia* lectin. J Biol Chem 278: 27059-27067, 2003.
35. Sumner JB, Howell SF and Zeissig A: Concanavalin a and Hemagglutination. Science 82: 65-66, 1935.
36. Rivera C: Essentials of oral cancer. Int J Clin Exp Pathol 8: 11884-11894, 2015.
37. Güneri P and Epstein JB: Late stage diagnosis of oral cancer: Components and possible solutions. Oral Oncol 50: 1131-1136, 2014.
38. Vokes EE: Induction chemotherapy for head and neck cancer: Recent data. Oncologist 15 (Suppl 3): S3-S7, 2010.
39. Marcazzan S, Varoni EM, Blanco E, Lodi G and Ferrari M: Nanomedicine, an emerging therapeutic strategy for oral cancer therapy. Oral Oncol 76: 1-7, 2018.
40. Furness S, Glenny AM, Worthington HV, Pavitt S, Oliver R, Clarkson JE, Macluskey M, Chan KK and Conway DI: Interventions for the treatment of oral cavity and oropharyngeal cancer: Chemotherapy. Cochrane Database Syst Rev 2011: CD006386, 2011.
41. Bonner JA, Harari PM, Giralt J, Azarnia N, Shin DM, Cohen RB, Jones CU, Sur R, Raben D, Jassem J, *et al*: Radiotherapy plus cetuximab for squamous-cell carcinoma of the head and neck. N Engl J Med 354: 567-578, 2006.
42. Vermorken JB, Mesia R, Rivera F, Remenar E, Kawecki A, Rottey S, Erfan J, Zabolotnyy D, Kienzer HR, Cupissol D, *et al*: Platinum-based chemotherapy plus cetuximab in head and neck cancer. N Engl J Med 359: 1116-1127, 2008.
43. Naruse T, Yanamoto S, Matsushita Y, Sakamoto Y, Morishita K, Ohba S, Shiraishi T, Yamada SI, Asahina I and Umeda M: Cetuximab for the treatment of locally advanced and recurrent/metastatic oral cancer: An investigation of distant metastasis. Mol Clin Oncol 5: 246-252, 2016.
44. Amit M, Yen TC, Liao CT, Chaturvedi P, Agarwal JP, Kowalski LP, Ebrahimi A, Clark JR, Kreppel M, Zöller J, *et al*: Improvement in survival of patients with oral cavity squamous cell carcinoma: An international collaborative study. Cancer 119: 4242-4248, 2013.
45. Takei J, Kaneko MK, Ohishi T, Kawada M, Harada H and Kato Y: H_2Mab-19, an anti-human epidermal growth factor receptor 2 monoclonal antibody exerts antitumor activity in mouse oral cancer xenografts. Exp Ther Med 20: 846-853, 2020.
46. Hanken H, Gaudin R, Gröbe A, Fraederich M, Eichhorn W, Smeets R, Simon R, Sauter G, Grupp K, Izbicki JR, *et al*: Her2 expression and gene amplification is rarely detectable in patients with oral squamous cell carcinomas. J Oral Pathol Med 43: 304-308, 2014.
47. Yan M, Schwaederle M, Arguello D, Millis SZ, Gatalica Z and Kurzrock R: HER2 expression status in diverse cancers: Review of results from 37,992 patients. Cancer Metastasis Rev 34: 157-164, 2015.
48. Kondo N, Ishiguro Y, Kimura M, Sano D, Fujita K, Sakakibara A, Taguchi T, Toth G, Matsuda H and Tsukuda M: Antitumor effect of gefitinib on head and neck squamous cell carcinoma enhanced by trastuzumab. Oncol Rep 20: 373-378, 2008.

49. Kondo N, Tsukuda M, Sakakibara A, Takahashi H, Hyakusoku H, Komatsu M, Niho T, Nakazaki K and Toth G: Combined molecular targeted drug therapy for EGFR and HER-2 in head and neck squamous cell carcinoma cell lines. Int J Oncol 40: 1805-1812, 2012.
50. Itai S, Ohishi T, Kaneko MK, Yamada S, Abe S, Nakamura T, Yanaka M, Chang YW, Ohba SI, Nishioka Y, *et al*: Anti-podocalyxin antibody exerts antitumor effects via antibody-dependent cellular cytotoxicity in mouse xenograft models of oral squamous cell carcinoma. Oncotarget 9: 22480-22497, 2018.
51. Kato Y and Kaneko MK: A cancer-specific monoclonal antibody recognizes the aberrantly glycosylated podoplanin. Sci Rep 4: 5924, 2014.
52. Yamada S, Ogasawara S, Kaneko MK and Kato Y: LpMab-23: A cancer-specific monoclonal antibody against human podoplanin. Monoclon Antib Immunodiagn Immunother 36: 72-76, 2017.
53. Kaneko MK, Yamada S, Nakamura T, Abe S, Nishioka Y, Kunita A, Fukayama M, Fujii Y, Ogasawara S and Kato Y: Antitumor activity of chLpMab-2, a human-mouse chimeric cancer-specific antihuman podoplanin antibody, via antibody-dependent cellular cytotoxicity. Cancer Med 6: 768-777, 2017.
54. Kaneko MK, Nakamura T, Kunita A, Fukayama M, Abe S, Nishioka Y, Yamada S, Yanaka M, Saidoh N, Yoshida K, *et al*: ChLpMab-23: Cancer-specific human-mouse chimeric anti-podoplanin antibody exhibits antitumor activity via antibody-dependent cellular cytotoxicity. Monoclon Antib Immunodiagn Immunother 36: 104-112, 2017.